Supporting Information

Two-dimensional N/O co-doped porous turbostratic carbon nanomeshes with expanded interlayer spacing as host material for potassium/lithium half/full batteries

Dongyang Qu[a,b]*, Bolin Zhao*[c]*, Zhongqian Song*[c]*, Dandan Wang*[d]*, Huijun Kong*[a,b]*, Shiyu Gan* [c]*, Yingming Ma*[c]*, Xiandui Dong*[ab]*, Dongxue Han**[c] *and Li Niu**[c]

[a] Ms. D. Y. Qu, Ms. H. J. Kong, Prof. X. D. Dong

State Key Laboratory of Electroanalytical Chemistry, c/o Engineering Laboratory for Modern Analytical Techniques, CAS Center for Excellence in Nanoscience, Changchun Institute of Applied Chemistry, Chinese Academy of Sciences, Changchun 130022, Jilin, P. R. China

[b] Ms. D. Y. Qu, Ms. H. J. Kong, Prof. X. D. Dong

University of Science and Technology of China, Hefei 230026, Anhui, P. R. China

[c] Mr. B. L. Zhao, Dr. Z. Q. Song, Dr. Y. M. Mang, Prof. S. Y. Gan, Prof. D. X. Han, Prof. L. Niu

Center for Advanced Analytical Science, c/o School of Chemistry and Chemical Engineering, Guangzhou University, Guangzhou 510006, P. R. China

[d] Dr. D. D. Wang

Key Laboratory of Functional Materials Physics and Chemistry of the Ministry of Education, College of Physics, Jilin Normal University, Changchun 130103, P. R. China

Emails: lniu@gzhu.edu.cn

Experimental section

Synthesis of 2D N/O co-doped carbon nanomeshes (NOPTCs)

All analytical grade chemical reagents were used as received without further purification. The precursor PU was prepared by the improved method.[1] Firstly, 20 mmol of urea and 20 mmol of 1, 4-Phenylene diisocyanate (PDI) were evenly dispersed in 200 ml acetone via ultrasonic vibration for 30 minutes and further continuously stirred for 10 hours at room temperature for complete polymerization. The obtained milky solution was disposed by vacuum filtration, washing with acetone for several times before drying under vacuum at 80 °C overnight.

The as-obtained white PU precursor was uniformly grinded in the agate mortar and then transferred into a tubular furnace, the reactor was heated to 600 °C for 3 hours and then to the target temperature T for 1 hour with a heating rate of 2 °C min^{-1} in the Ar atmosphere to convert into NOPTCs-T (T=600, 700 and 800 °C).

Materials characterization

Field-emission scanning electron microscope (SEM, Philips XL 30) and transmission electron microscope (TEM, Hatachi 600) with an energy-dispersive X-ray spectrometer (EDS, Bruker Quantax) were employed to observe morphology and microstructure of the resulting products. The structure of the carbon materials was investigated by powder X-ray diffraction (XRD, BRUKERD/MAX 2500 V/PV) with Cu K_α radiation in the 2θ range of 10–80° and Raman spectra (Renishaw 2000). Fourier transform infrared spectrometry was carried out using a Brucker TENSOR II. X-ray photoelectron spectroscopy (XPS) measurements were tested to characterize the components and valence state of the elements by VG Thermo ESCALAB 250 spectrometer (VG Scientific) operated at 120 W. The nitrogen adsorption-desorption isotherms (BET, Autosorb iQ Station 2) were performed to indicate the specific surface areas and porous texture properties at 77 K using N_2 as the adsorbate.

Electrochemical measurements

The as-prepared carbon materials, the conductive agent (acetylene black) and the binder (Carboxyl methyl Cellulose, CMC) were uniformly mixed with a weight ratio of 7:2:1 in distilled water. The resulting slurry was then homogeneous coated on a Cu foil collector and dried in a vacuum at 60 °C for 12 h. The cathode slurry of PIBs/LIBs was obtained by mixing 70 wt% of potassium Prussian blue nanoparticles (KPB)/$LiFePO_4$, 20 wt% of acetylene black and 10 wt% of polyvinylidene fluoride in N-methyl-2-pyrrolidinone and coated an Al foil, dried at 110 °C for 12 h in vacuum condition. The CR2032 coin-type half-cell and full-cell was assembled in an argon-filled glove box with both moisture and oxygen concentrations below 0.01 ppm. For the PIBs, 3M KFSI in dimethoxyethane (DME) was used as the electrolyte, the pure K foil was acted as both the reference electrode and counter electrode, and the glass microfiber filter (934-AH, Whatman) was used as the separator. For the LIBs, a solution of 1 M $LiPF_6$ in ethylene carbonate (EC) and diethyl carbonate (DEC) (1:1 by volume) was used as the electrolyte, the pure Li foil was regarded as both the reference electrode and counter electrode, and the glass microfiber filter (934-AH, Whatman) was used as the separator. The galvanostatic charge/discharge tests were performed on LAND-CT2001A with a voltage range of 0.01 to 3 V. A sequence of cyclic voltammetry (CV) curves were conducted at different scanning rates on an electrochemical workstation (CHI 660C, Chenhua), and the electrochemical impedance spectroscopy (EIS) was recorded on a frequency range of 100 kHz to 0.01 Hz. The galvanostatic intermittent titration technique (GITT) was tested by applying a current density of 50 mA g^{-1} with current pulse duration for 0.5 h followed by relaxation intervals of 2 h.

Theoretical Calculation

All the density functional theory (DFT) simulations were implemented in The Vienna Ab Initio Package (VASP) within the generalized gradient approximation (GGA) using the Perdew–Burke–Ernzerhof (PBE) exchange-correction formulation. The periodic super-cells including 5 × 5 unit cells was employed to model carbon, N-doped carbon and N/O co-doped carbon systems, as well as all atoms were in a state of relaxation during structural optimization. The Kohn-Sham orbitals were enlarged in a plane wave basis set with a kinetic energy cutoff of 450 eV to associate with valence electrons.

The adsorption energy per K atom (E_{ads}) was defined by the following equation:

$E_{\mathrm{ads}} = E_{\mathrm{total}} - E_{\mathrm{str}} - E_{\mathrm{K}}$

where E_{total}, E_{str} and E_{K} are the total energy of K atom attached to the graphene surface, the energy of a bare structure without K, and half of the energy of the body center cubic K unit cell, respectively.

The electron density difference was calculated by subtracting the charge densities of K atoms and configuration from the corresponding models. The density of states (DOS) for the electronic relaxation was calculated by using 15 × 15 × 1 Gamma mesh. The K-ions diffusion energy barriers on three models were calculated with the complete LST/QST method.

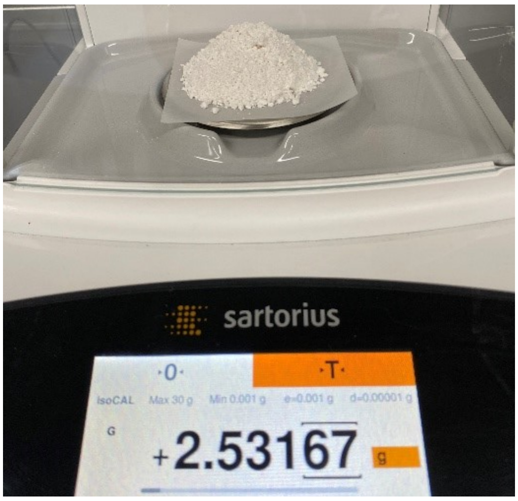

Figure S1. Photograph of the high yield PU precursors.

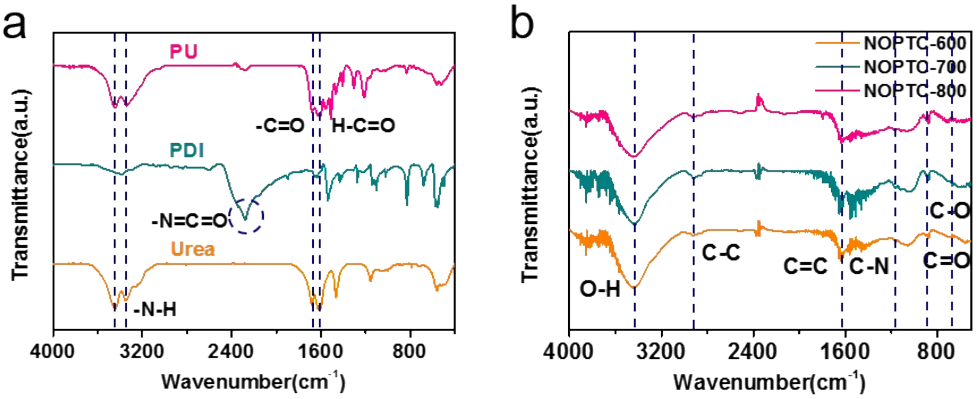

Figure S2. a) FTIR spectra of urea, PDI and PU. b) FTIR spectra of three samples.

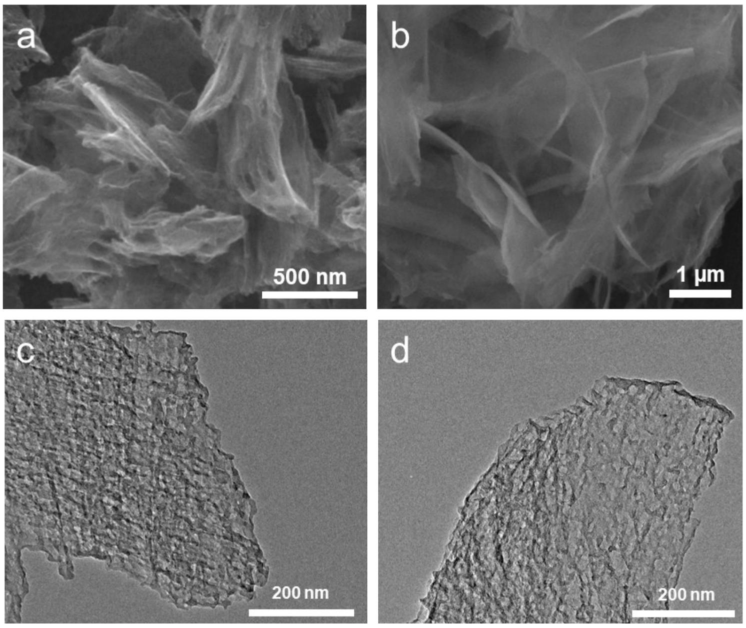

Figure S3. SEM and TEM images of a,c) NOPTC-600 and b,d) NOPTC-800 materials.

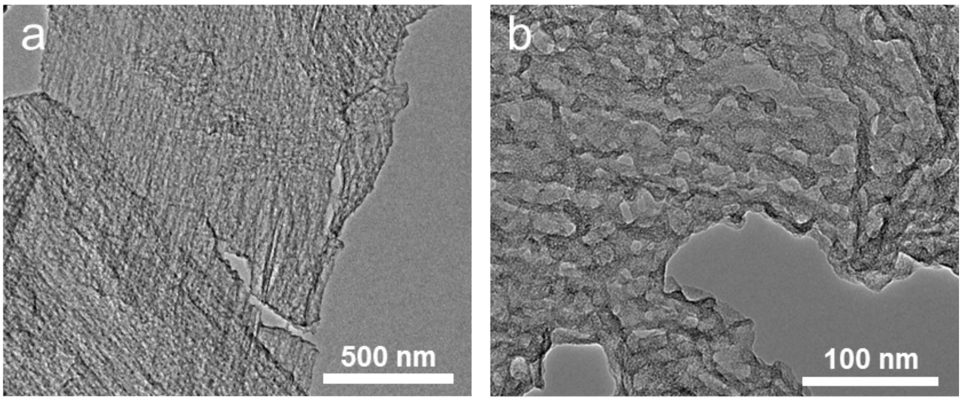

Figure S4. a,b)TEM image of NOPTC-700 at different scale bar.

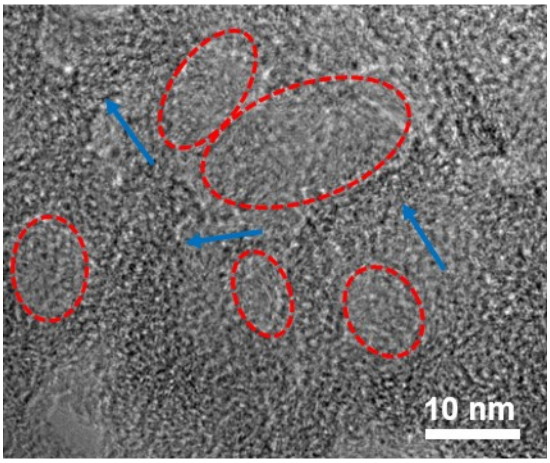

Figure S5. HRTEM image of NOPTC-700 (red circle: mesopore; blue arrow: turbostratic stacked carbon layer).

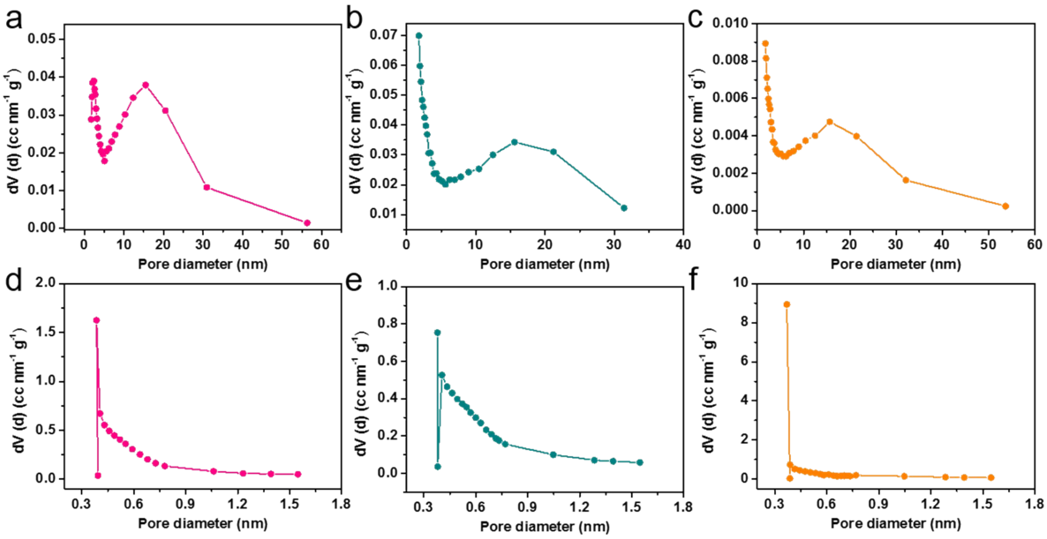

Figure S6. The BJH and HK pore size distribution curves of a, d) NOPTC-600, b,e) NOPTC-700 and c, f) NOPTC-800.

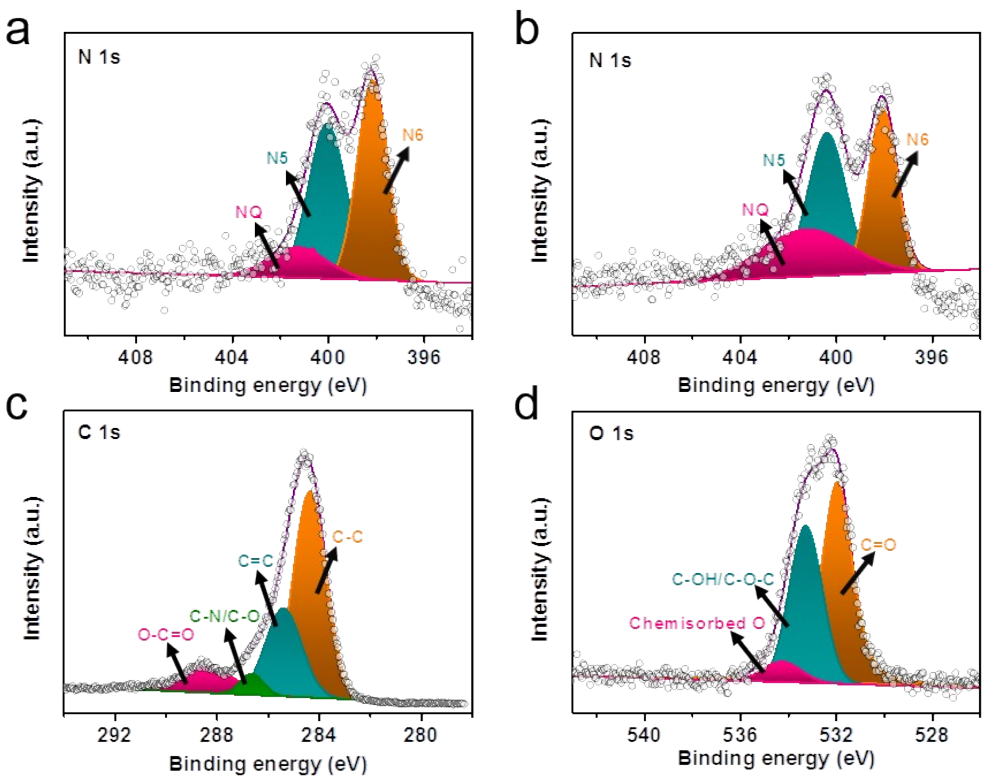

Figure S7. High-resolution N 1s XPS spectrum of a) NOPTC-600 and b) NOPTC-800. High-resolution XPS c) C 1s and d) O 1s spectrum of NOPTC-700.

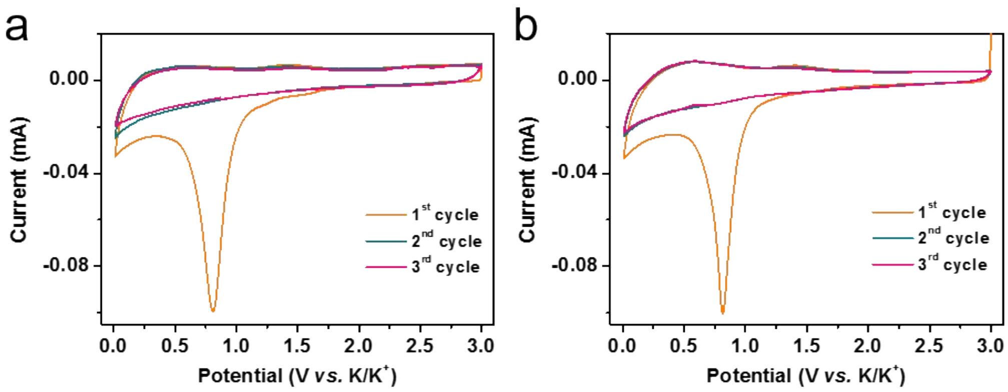

Figure S8. CV curves of a) NOPTC-600 and b) NOPTC-800 at a scan rate of 0.1 mV s^{-1}.

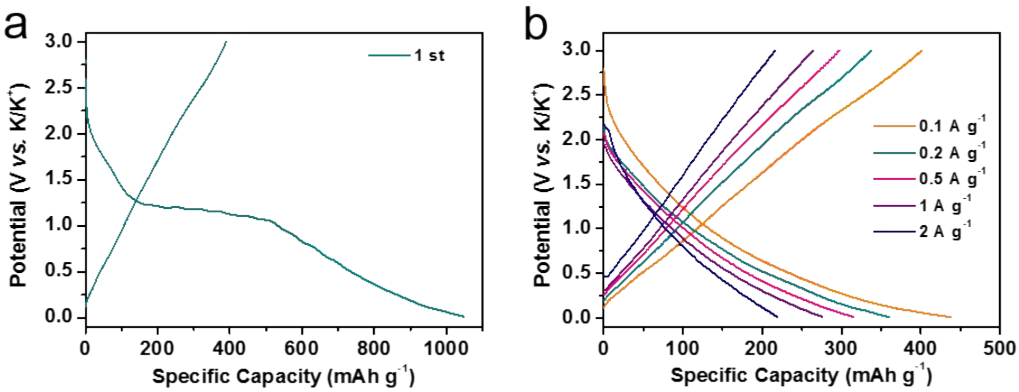

Figure S9. The potassiation and depotassiation profiles of the NOPTC-700 a) for the first cycles at 0.1 A g^{-1} and b) at different current densities.

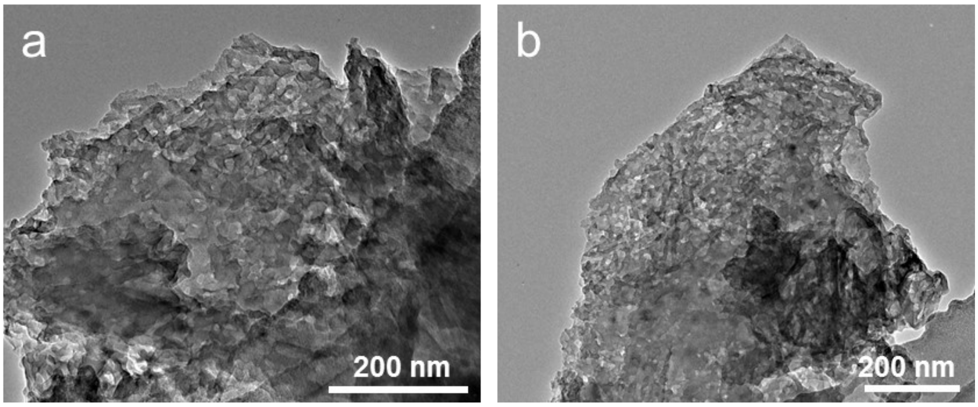

Figure S10. TEM image of the NOPTC-700 after a) 200 cycles at 0.1 A g^{-1} and b) 500cycles at 1 A g^{-1}.

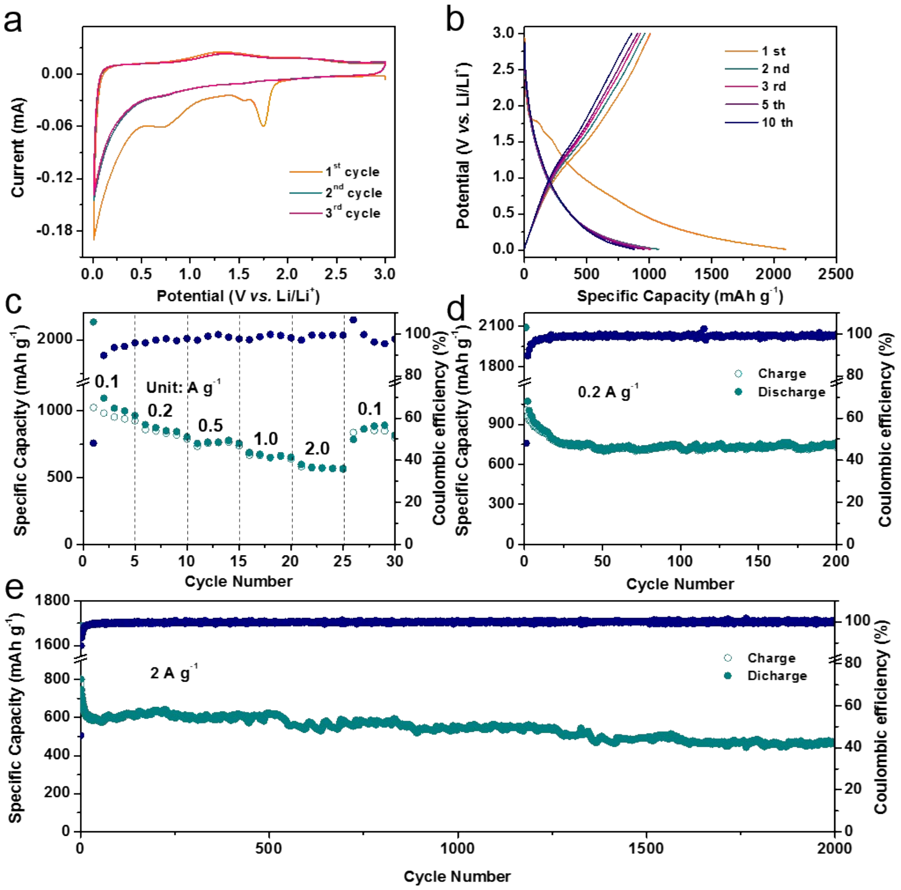

Figure S11. Electrochemical properties of obtained NOPTC-700 as LIBs anode. a) CV curves for three cycles at 0.1 mV s^{-1}. b) GCD profiles curves for the 1st, 2nd, 3rd, 5th, and 10th cycles under at 0.2 A g^{-1}. c) Rate capability of the NOPTC-700 and d) Cycling performance at 0.2 A g^{-1}. e) Ultralong cycle stability and Coulombic efficiency of NOPTC-700 at 2A g^{-1}.

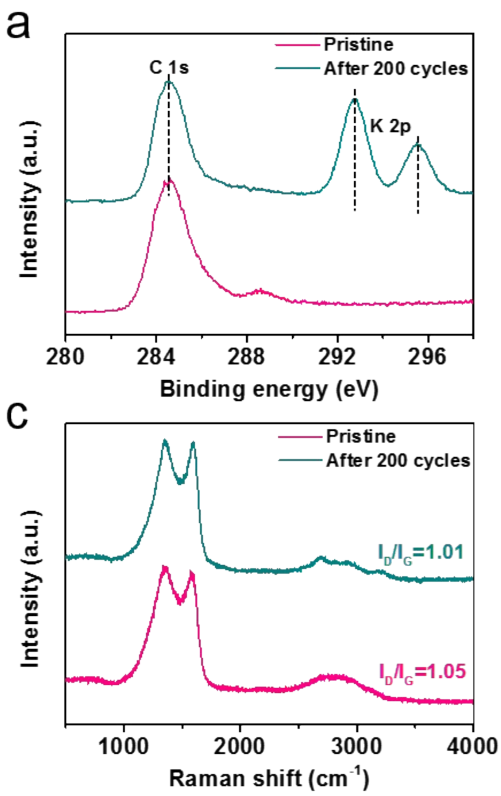

Figure S12. Comparison of a). High resolution C 1s and K 2p spectra, b) XRD patterns, c) Raman and d) FTIR spectrum of NOPTC-700 before and after 200 cycles at 1 A g^{-1}.

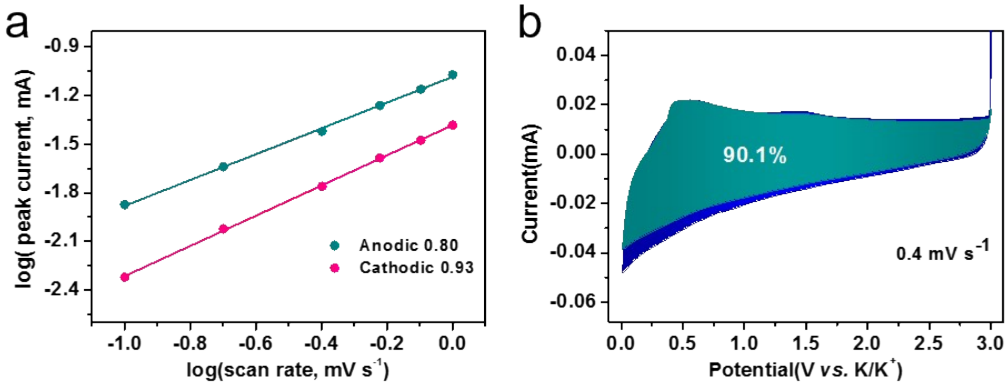

Figure S13. a) Relationship between log *v* and log *i* at anodic and cathodic peak currents. b) Capacitive contribution from the CV curve at a scan rate of 0.4 mv (green area).

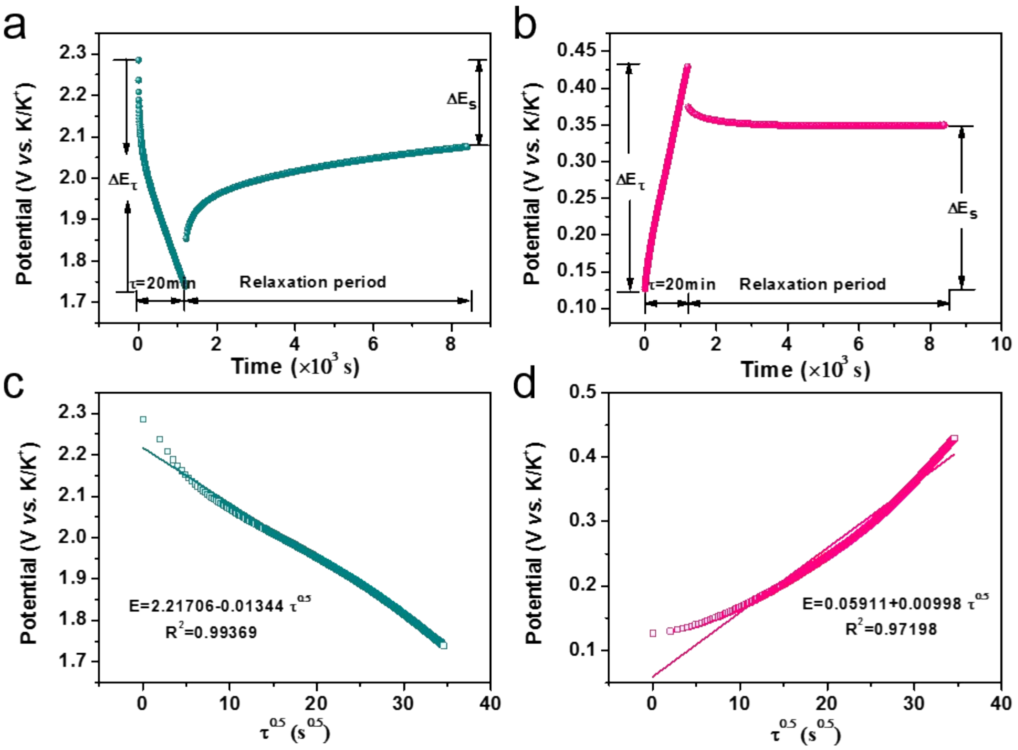

Figure S14. a) Galvanostatic intermittent titration technique (GITT) profiles of NOPTC-700 after five cycles. A single GITT curve for discharge and charge process. τ vs. E profiles for a single GITT titration during b) Discharge and d) Charge processes. The corresponding linearly fitting behavior of E vs. τ 1/2 for the c) Discharge and e) Charge GITT titration.

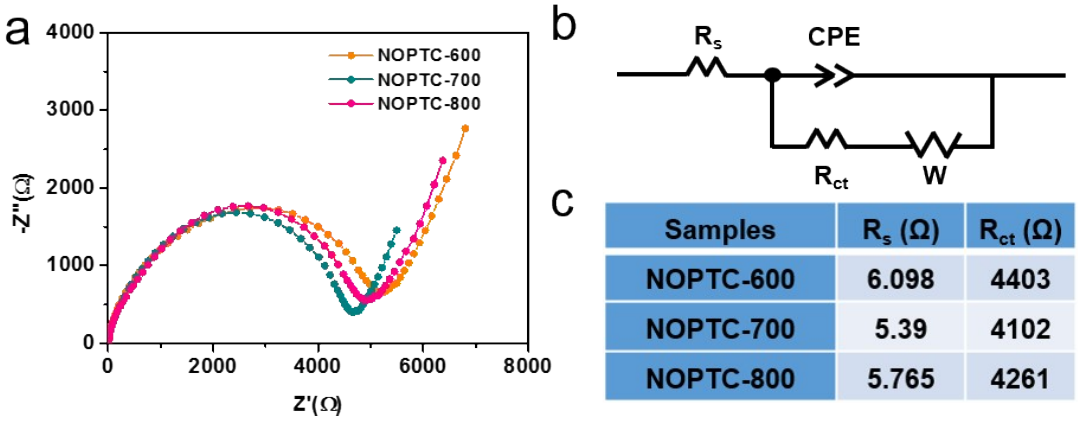

Samples	R$_s$ (Ω)	R$_{ct}$ (Ω)
NOPTC-600	6.098	4403
NOPTC-700	5.39	4102
NOPTC-800	5.765	4261

Figure S15. a). EIS spectra of the three samples. b) The Randles equivalent circuit model. c) The EIS fitting parameters of the three samples.

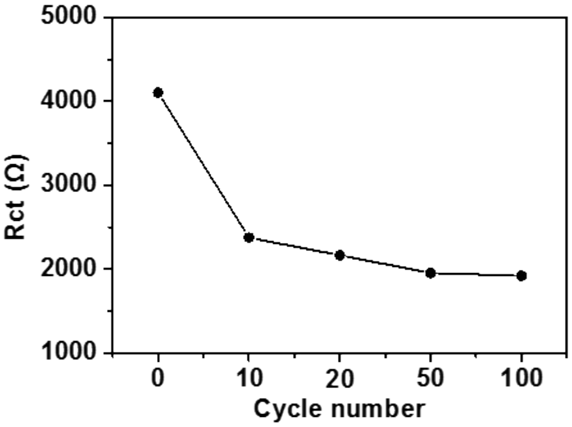

Figure S16. The fitting charge-transfer resistance (R_{ct}) of NOPTC-700 electrode after different cycles.

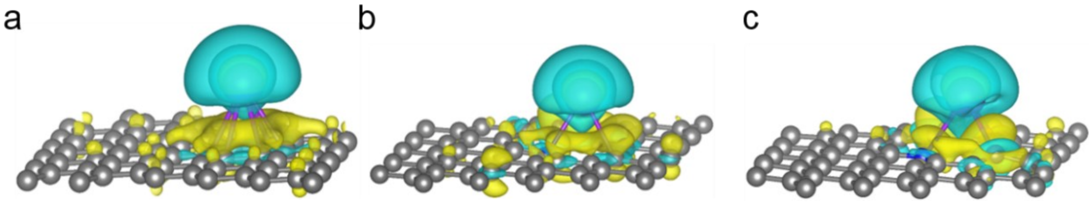

Figure S17. Electron density differences of K ion adsorbed in the a) Carbon, b) N-doped carbon and c) N/O co-doped carbon (0.001 e/bohr3).

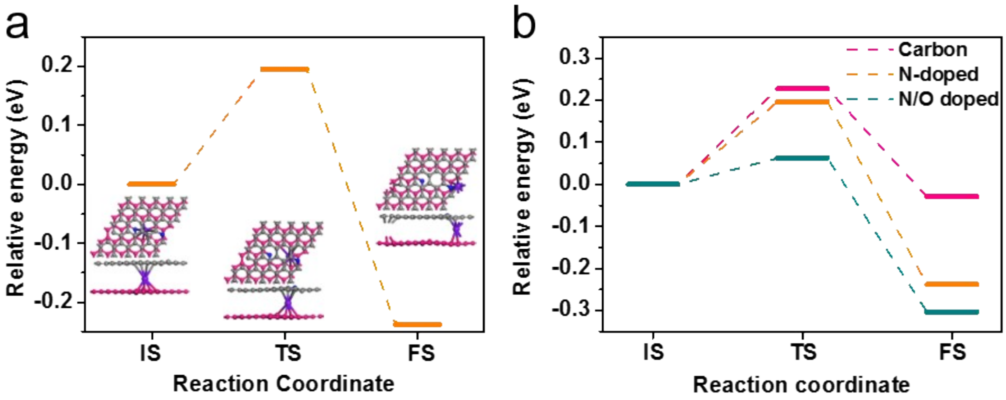

Figure S18. K-ions diffusion energy barriers in a) N-doped carbon and b) Three models.

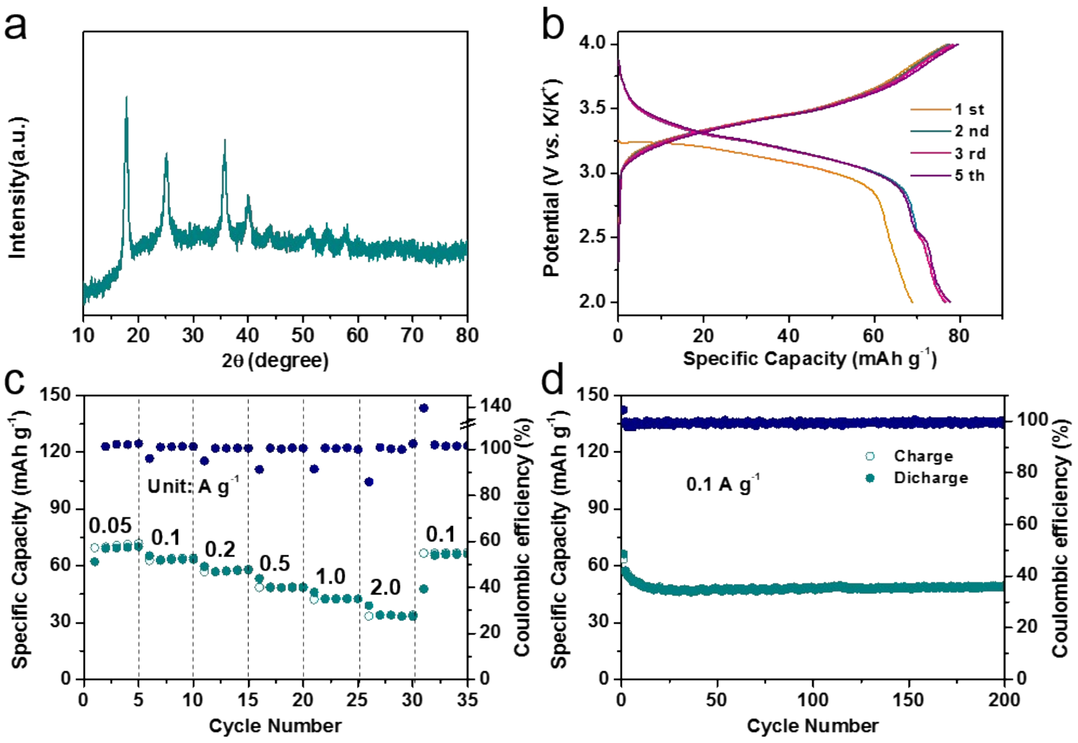

Figure S19. a) XRD pattern. b) GCD profiles. c) Rate performance and d) Cycling stability at 0.1 A g^{-1} of the KPB cathode material.

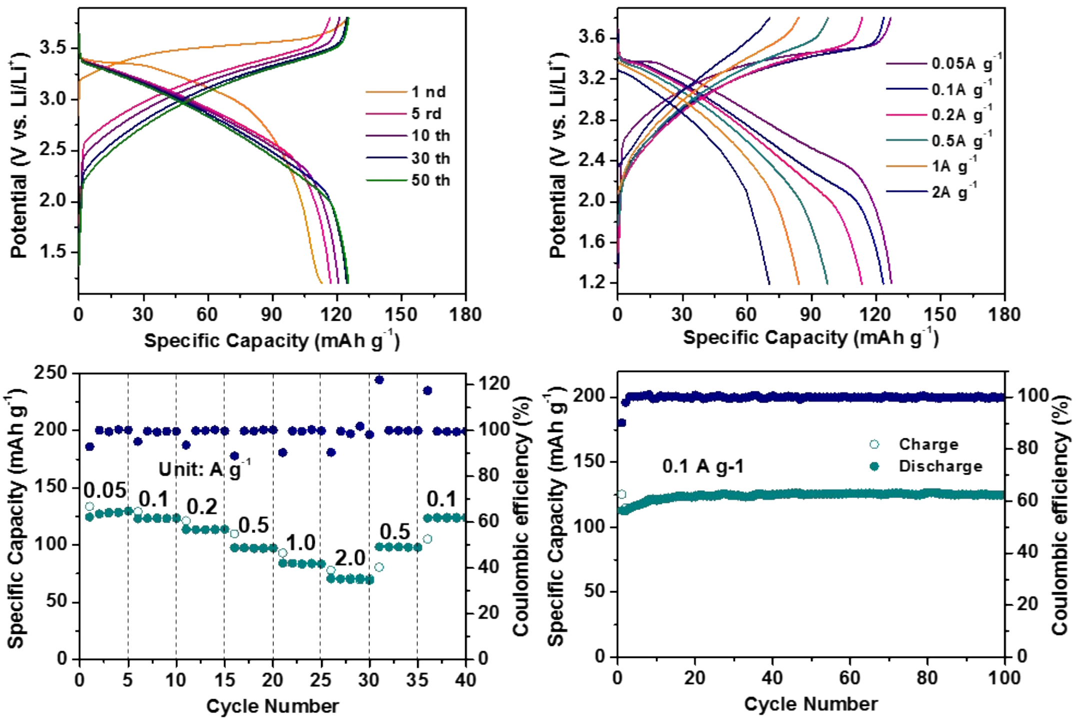

Figure S20. Li-storage properties of LFP//NOPTC-700 full cells. GCD profiles of the full cell at different a) Cycles. and c) Current densities. b) Rate capability and d)

Cycling stability at 0.1 A g^{-1}.

Table S1. The pore volumes of mesopores and micropores of three samples.

Samples	**pore volumes of mesopores (cm^3/g)**	**pore volumes of micropores (cm^3/g)**
NOPTC-600	1.211	0.231
NOPTC-700	1.342	0.239
NOPTC-800	1.715	0.246

Table S2. Elemental composition determined by XPS of the different NOPTC-*T*.

Samples	**C（at%）**	**N（at%）**	**O（at%）**
NOPTC-600	79.30	7.78	12.89
NOPTC-700	82.43	7.63	9.94
NOPTC-800	85.74	7.52	6.74

Table S3. Chemical configuration of N 1s and the corresponding percentage.

Samples	**NQ (%)**	**N5 (%)**	**N6 (%)**
NOPTC-600	12.8	42.3	44.9
NOPTC-700	23.9	35.6	40.4
NOPTC-800	29.1	34.1	36.8

Table S4. Comparison of PIBs performance of the NOPTC-700 with previously reported literature.

Materials	**Capacity**	**Cyclability**	**Reference**
NOPTC-700	437.1 mAh g^{-1} at 0.1 A g^{-1} 219.0 mAh g^{-1} at 2 A g^{-1}	400.4 mAh g^{-1}, 100 Cycles (0.1 A g^{-1}) 292.8 mAh g^{-1} , 100 Cycles (1 A g^{-1})	This work
HPNCFs	197 mAh g^{-1} at 0.05 A g^{-1} 57 mAh g^{-1} at 0.25 A g^{-1}	65 mAh g^{-1}, 346 cycles (0.1 A g^{-1})	[2]

MCOs	354 mAh g^{-1} at 0.05 A g^{-1} 110 mAh g^{-1} at 1 A g^{-1}	100 mAh g^{-1}, 1300 cycles (1 A g^{-1})	3
GNCs	369 mAh g^{-1} at 0.05 A g^{-1} 152 mAh g^{-1} at 1 A g^{-1}	189 mAh g^{-1}, 200 cycles (0.2 A g^{-1})	4
CHMBs	377 mAh g^{-1} at 0.1 A g^{-1} 182 mAh g^{-1} at 2 A g^{-1}	133 mAh g^{-1}, 1000 cycles (1 A g^{-1})	5
N-HPC	292 mAh g^{-1} at 0.1 A g^{-1} 94 mAh g^{-1} at 10 A g^{-1}	204 mAh g^{-1}, 1000 cycles (0.5 A g^{-1})	6
NOHC	304.6 mAh g^{-1} at 0.1 A g^{-1} 178.9 mAh g^{-1} at 5 A g^{-1}	189.5 mAh g^{-1} , 5000 cycles (1 A g^{-1})	7
N,P-VG@CC	303.6 mAh g^{-1} at 0.05 A g^{-1} 180.6 mAh g^{-1} at 1 A g^{-1}	142.4 mAh g^{-1} , 1000 cycles (1 A g^{-1})	8
NCNFs	280 mAh g^{-1} at 0.1 A g^{-1} 170 mAh g^{-1} at 5 A g^{-1}	150 mAh g^{-1}, 5000 cycles (5 A g^{-1})	9
CMSs	328 mAh g^{-1} at 0.1 A g^{-1} 150 mAh g^{-1} at 5 A g^{-1}	1360 mAh g^{-1}, 10000 cycles (2 A g^{-1})	10
ENPCS	276 mAh g^{-1} at 0.05 A g^{-1} 157 mAh g^{-1} at 2 A g^{-1}	183 mAh g^{-1}, 137 cycles (1 A g^{-1})	11
PN-PCM	453 mAh g^{-1} at 0.05 A g^{-1} 168 mAh g^{-1} at 10 A g^{-1}	218 mAh g^{-1}, 3000 cycles (1 A g^{-1})	12
S-MCCF	388.2 mAh g^{-1} at 0.05 A g^{-1} 182.7 mAh g^{-1} at 5 A g^{-1}	150 mAh g^{-1}, 2000 cycles (1 A g^{-1})	13
TWC-SC-G	364 mAh g^{-1} at 0.03 A g^{-1} 223 mAh g^{-1} at 1 A g^{-1}	235 mAh g^{-1}, 1000 cycles (1 A g^{-1})	14
NCF	282.8 mAh g^{-1} at 0.05 A g^{-1} 108.3 mAh g^{-1} at 2 A g^{-1}	104.3 mAh g^{-1}, 300 cycles (1 A g^{-1})	15
CACF	350.5 mAh g^{-1} at 0.1 A g^{-1} 152.7 mAh g^{-1} at 10 A g^{-1}	201.5 mAh g^{-1}, 5000 cycles (2 A g^{-1})	16

Notes and references

1. Q. Lai, J. Zheng, Z. Tang, D. Bi, J. Zhao and Y. Liang, *Angew. Chem. Int. Ed.*, 2020, **59**, 11999-12006.
2. M. Zhang, M. Shoaib, H. Fei, T. Wang, J. Zhong, L. Fan, L. Wang, H. Luo, S. Tan, Y. Wang, J. Zhu, J. Hu and B. Lu, *Adv. Energy Mater.*, 2019, **9**, 1901663.
3. G. Xia, C. Wang, P. Jiang, J. Lu, J. Diao and Q. Chen, *J. Mater. Chem. A*, 2019, **7**, 12317-12324.
4. W. Zhang, J. Ming, W. Zhao, X. Dong, M. N. Hedhili, P. M. F. J. Costa and H. N. Alshareef, *Adv. Funct. Mater.*, 2019, **29**, 1903641.
5. Z. Zhang, B. Jia, L. Liu, Y. Zhao, H. Wu, M. Qin, K. Han, W. A. Wang, K. Xi, L. Zhang, G. Qi, X. Qu and R. V. Kumar, *ACS Nano*, 2019, **13**, 11363-11371.
6. X. Zhou, L. Chen, W. Zhang, J. Wang, Z. Liu, S. Zeng, R. Xu, Y. Wu, S. Ye, Y. Feng, X. Cheng, Z. Peng, X. Li and Y. Yu, *Nano Lett.*, 2019, **19**, 4965-4973.
7. R. C. Cui, B. Xu, H. J. Dong, C. C. Yang and Q. Jiang, *Adv Sci (Weinh)*, 2020, **7**, 1902547.
8. W. Qiu, H. Xiao, Y. Li, X. Lu and Y. Tong, *Small*, 2019, DOI: 10.1002/smll.201901285, 1901285.
9. F. Liu, J. Meng, F. Xia, Z. Liu, H. Peng, C. Sun, L. Xu, G. Van Tendeloo, L. Mai and J. Wu, *J. Mater. Chem. A*, 2020, **8**, 18079-18086.
10. J. Ge, B. Wang, J. Zhou, S. Liang, A. M. Rao and B. Lu, *ACS Materials Letters*, 2020, **2**, 853-860.
11. F. Xu, Y. Zhai, E. Zhang, Q. Liu, G. Jiang, X. Xu, Y. Qiu, X. Liu, H. Wang and S. Kaskel, *Angew. Chem. Int. Ed.*, 2020, **59**, 19460-19467.
12. J. Gong, G. Zhao, J. Feng, Y. An, T. Li, L. Zhang, B. Li and Z. Qian, *ACS Nano*, 2020, **14**, 14057-14069.
13. Y. Xu, J. Ruan, Y. Pang, H. Sun, C. Liang, H. Li, J. Yang and S. Zheng, *Nano-Micro Letters*, 2020, **13**.
14. Z. Tang, Y. Wang, Z. Zheng and X. Luo, *J. Mater. Chem. A*, 2021, **9**, 9191-9202.

15. L. Li, Y. Li, Y. Ye, R. Guo, A. Wang, G. Zou, H. Hou and X. Ji, *ACS Nano*, 2021, **15**, 6872-6885.

16. M. Chen, W. Liu, Y. Du, Y. Cui, W. Feng, J. Zhou, X. Gao, T. Wang, S. Liu and Y. Jin, *ACS Sustainable Chem. Eng.*, 2021, **9**, 3931-3941.